Mapping Complex Tissue Architecture With Diffusion Spectrum Magnetic Resonance Imaging

Van J. Wedeen,[1*] Patric Hagmann,[2,3] Wen-Yih Isaac Tseng,[4] Timothy G. Reese,[1] and Robert M. Weisskoff[1]

Methods are presented to map complex fiber architectures in tissues by imaging the 3D spectra of tissue water diffusion with MR. First, theoretical considerations show why and under what conditions diffusion contrast is positive. Using this result, spin displacement spectra that are conventionally phase-encoded can be accurately reconstructed by a Fourier transform of the measured signal's modulus. Second, studies of in vitro and in vivo samples demonstrate correspondence between the orientational maxima of the diffusion spectrum and those of the fiber orientation density at each location. In specimens with complex muscular tissue, such as the tongue, diffusion spectrum images show characteristic local heterogeneities of fiber architectures, including angular dispersion and intersection. Cerebral diffusion spectra acquired in normal human subjects resolve known white matter tracts and tract intersections. Finally, the relation between the presented model-free imaging technique and other available diffusion MRI schemes is discussed. Magn Reson Med 54:1377–1386, 2005. © 2005 Wiley-Liss, Inc.

Over the past decade, MRI methods have been developed that can nondestructively map the structural anisotropy of fibrous tissues in living systems by mapping the diffusion tensor (DT) of tissue water (for review see Ref. 1). Such methods have been used to elucidate the fiber architecture and functional dynamics of the myocardium (2,3) and skeletal muscle (4). They have also been used in the nervous system to identify and map the trajectories of neural white matter tracts and infer neuroanatomic connectivity (for review see Ref. 5).

Notwithstanding this progress, the DT paradigm has notable limitations. Because the distances resolved by MRI are far larger than the diffusion scale, each 3D resolution element (voxel) represents many distinct diffusional environments. This provides a complicated diffusion signal that in general is underspecified by the six degrees of freedom of the DT model. An example of particular interest occurs when a tissue has a composite fiber structure, such that each small region may contain fibers of multiple orientations corresponding to distinct diffusion anisotropies (6).

The present study describes a model-free MRI methodology called diffusion spectrum imaging (DSI). This method affords the capacity to resolve intravoxel diffusion heterogeneity of compartments with sufficient angular separation and anisotropy by measuring its diffusion density spectra estimator. In describing this method, we will show that DSI generalizes the analysis of diffusion spectra by demonstrating that the Fourier transform of the diffusion spectrum must be positive. We also discuss how the DSI method encompasses existing alternate analyses of MRI diffusion contrast, and present examples of diffusion contrast in biological tissues analyzed with DSI.

THEORY

Measuring the Diffusion Spectrum

We consider the classical Stejskal-Tanner experiment (7). It allows the phase-encoding of spin displacements by embedding a strong pulse gradient of duration δ and intensity $|\mathbf{g}|$ on each side of the π RF-pulse of a conventional spin-echo sequence. In such a manner the MR signal is made proportional to the voxel average ($\langle \cdot \rangle$) dephasing for a specified diffusion duration Δ, which is the time elapsed between the beginning of the first and second diffusion gradients

$$S_\Delta = S_0 \langle e^{i\phi} \rangle. \quad [1]$$

where S_0 is a constant that can be computed by the spin-echo experiment without diffusion weighting. To gain some insight about Eq. [1], we assume at first instance that the duration δ of the diffusion sensitizing gradient is negligible compared to the mixing time Δ (8). Thanks to this narrow pulse approximation, the dephasing becomes proportional to the scalar product between the relative spin displacement $\mathbf{r}$ and the gradient wave vector $\mathbf{q}$. Thus we have $\phi = \mathbf{q} \cdot \mathbf{r}$ with $\mathbf{r} = \mathbf{x}(\Delta) - \mathbf{x}(0)$. $\mathbf{x}(0)$ and $\mathbf{x}(\Delta)$ must be understood as the spin position at the time of the application of the first and second diffusion gradient pulses, respectively. The gradient wave vector is defined as $\mathbf{q} = \gamma\delta\mathbf{g}$, where γ is the gyromagnetic ratio and $\mathbf{g}$ is the gradient vector.

We can consider the voxel average as an expectation $E(\cdot)$, which implies that the MR signal is proportional to the characteristic function (9) of the relative spin displacement vector. This yields a Fourier relationship between the MR signal and the underlying density $\bar{p}_\Delta(\mathbf{r})$.

[1]Department of Radiology, MGH Martinos Center for Biomedical Imaging, Harvard Medical School, Charlestown, Massachusetts, USA.

[2]Department of Radiology, University Hospital (CHUV), Lausanne, Switzerland.

[3]Signal Processing Institute, École Polytechnique Fédérale de Lausanne (EPFL), Lausanne, Switzerland.

[4]Center for Optoelectronic Biomedicine, National Taiwan University College of Medicine, Taipei, Taiwan.

Grant sponsor: National Institutes of Health; Grant number: NIH 1 R01-MH64044; Grant sponsors: Swiss National Science Foundation; Mr. Yves Paternot.

*Correspondence to: Dr. Van J. Wedeen, MGH Martinos Center for Biomedical Imaging, 149 13th St., 2nd floor, Charlestown, MA 02129. E-mail: van@nmr.mgh.harvard.edu.

Received 29 December 2004; revised 28 May 2005; accepted 2 June 2005.
DOI 10.1002/mrm.20642
Published online 24 October 2005 in Wiley InterScience (www.interscience.wiley.com).

$$S_\Delta(\mathbf{q}) = S_0 E(e^{i\phi}) \quad [2]$$

$$= S_0 \int_{\mathbb{R}^3} \bar{p}_\Delta(\mathbf{r}) e^{i\mathbf{q}\mathbf{r}} d^3\mathbf{r} \quad [3]$$

$\bar{p}_\Delta(\mathbf{r})$represents the density of the average relative spin displacement in a voxel (8). In other words, $\bar{p}_\Delta(\mathbf{r})d^3\mathbf{r}$ is a measure of the probability for a spin in a considered voxel to make, during the experimental mixing time Δ, a vector displacement $\mathbf{r}$. In the case of absence of net translation or flux, it describes the voxel averaged diffusion process. Of course, some care must be taken with this description because the signal is also potentially weighted by different MR susceptibility effects. Therefore, and because it is calculated by Fourier transformation of a measured quantity, we simply refer to $\bar{p}_\Delta(\mathbf{r})$ as the diffusion spectrum.

Practically, to exclude phase shifts arising from tissue motion, diffusion spectra are reconstructed by taking the Fourier transform of the modulus of the complex MR signal:

$$\bar{p}_\Delta(\mathbf{r}) = S_0^{-1}(2\pi)^{-3} \int_{\mathbb{R}^3} |S_\Delta(\mathbf{q})| e^{-i\mathbf{q}\mathbf{r}} d^3\mathbf{q} \quad [4]$$

Significantly, this modulus is precisely the information required to reconstruct the diffusion spectra. Indeed, the diffusion contrast (i.e., the Fourier transform of the diffusion spectrum) is positive. To be more precise we show in the sequel that the MRI signal is positive for any type of spin motion without net flux (i.e., spin displacements due to diffusion (thermal molecular agitation), or other random fluxes such as intravoxel incoherent motion (10)).

Why Diffusion Contrast is Positive

To show that diffusion contrast is positive, we need to assume that we are studying an isolated system with time-invariant properties in which no net fluxes occur. These conditions are well suited to our problem. The typical MR experiment achieves a voxel size of a few millimeters on each axis, and experimental mixing times on the order of tens of milliseconds. The influence of diffusion on the MR signal is proportional to the mass transfer. We combine these observations with the fact that the mass transfer is upper bounded by the case in which water diffuses freely. This means that in the extreme worst case, the mass that would transfer from one voxel to another during the acquisition of one diffusion direction is less than a few percent of the total voxel mass. In such situation the isolated system condition seems acceptable. In addition, we require that for the considered experimental time interval, which corresponds to the duration necessary to sample one diffusion direction, the system properties remain constant (e.g., local diffusion coefficients and compartment sizes do not change during the acquisition time $\Delta + \delta$). Accordingly, we consider the voxel as an isolated (or closed) system with diffusion properties that are time-invariant (i.e., homogenous). It remains for us to show that in a closed system the Fourier transform of a displacement spectrum due to a homogenous diffusion process in the stationary state is real and positive.

Problem Formulation

We model water diffusion in a voxel by the random walk of spins on a finite network, where the N vertices correspond to a sufficient number of compartments and the edges to the connection between them. We generally assume that there exists a path from any compartment to any other compartment (i.e., there is no isolated subnetwork, and thus we say that the network is irreducible) and we also assume that the system is driven only by diffusion (i.e., at equilibrium there is no net flow between any two compartments).

We construct the network with a complete directed graph of order N and associate to every vertex i:

- a position vector $\mathbf{x}_i \in \mathbb{R}^3$,
- a spin mass or number $\mu_i(t)$, which we define without loss of generality to be normalized: $\Sigma_i\, \mu_i(t) = 1$ for all $t \in \mathbb{R}^+$.

To each edge $i \to j$, we associate a weight q_{ij} that can be considered as the average mass transfer from compartment to compartment per unit time and per unit mass in i (or simply flux rate from i to j). The matrix $\mathbf{Q} = (q_{ij})_{ij}$ is a set of numbers that fully characterizes the system properties by incorporating all of the effects that influence spin transfer, such as local diffusion coefficients, local compartment volumes, and geometries.

Let the stochastic process $\{\mathbf{x}(t)\}_{t>0}$ with values in $\{\mathbf{x}_1, \ldots, \mathbf{x}_N\}$ be a random walk of a particle on that network.

Diffusion Process as a Markov Chain (MC)

In the MC formalism (9), the stochastic process $\{\mathbf{x}(t)\}_{t>0}$ can be understood as a regular jump continuous-time homogeneous MC of finite state space. Accordingly, the mass distribution vector, $\boldsymbol{\mu}(t) \triangleq [\mu_1(t), \ldots, \mu_N(t)]^T$, which we sometimes also write as a diagonal matrix $\mathbf{M} \triangleq \mathrm{diag}\{\mu_1(t), \ldots, \mu_N(t)\}$, becomes the distribution of the MC, whereas the flux rate matrix $\mathbf{Q}$ becomes its infinitesimal generator. The diffusion process is guided by a system of differential equations that is expressed by Kolmogorov's differential system (9). Its solution shows how the transition matrix $\mathbf{P}_t$ can be expressed in terms of $\mathbf{Q}$:

$$\mathbf{P}_t = e^{t\mathbf{Q}}. \quad [5]$$

$\{\mathbf{P}_t\}_{t>0}$is called the transition semigroup of the chain and corresponds for our system to the family of operators that drive the diffusion process. In other words, $\mathbf{P}_t$ is responsible for the evolution of the mass distribution vector $\boldsymbol{\mu}(s)$ along time:

$$\boldsymbol{\mu}^T(s+t) = \boldsymbol{\mu}^T(s)\mathbf{P}_t, \text{ with } t, s \in \mathbb{R}^+. \quad [6]$$

From the problem formulation we see that this MC is irreducible and ergodic (9), and consequently admits a unique stationary distribution $\boldsymbol{\pi} \triangleq [\pi_1, \ldots, \pi_N]^T$ (9). Moreover, we have assumed that diffusion is characterized

by the absence of net flux. In MC terminology, this means that the stationary distribution must satisfy the detailed balance equations, i.e., $\pi_i q_{ij} = \pi_j q_{ji}$. These equations can also be expressed by saying that $\mathbf{Q}$ has a similar matrix $\tilde{\mathbf{Q}}$ that is symmetric:

$$\mathbf{Q} = \mathbf{\Pi}^{-1/2}\tilde{\mathbf{Q}}\mathbf{\Pi}^{1/2}, \quad [7]$$

where $\mathbf{\Pi} \triangleq \text{diag}\{\pi_1, \ldots, \pi_N\}$. Similar matrices have identical eigenvalues (11) and symmetric matrices have real eigenvalues (11); therefore, $\mathbf{Q}$ and $\tilde{\mathbf{Q}}$ have identical and real eigenvalues that are $\mathbf{\Lambda} \triangleq \text{diag}\{\lambda_1, \ldots, \lambda_N\}$. If $\tilde{\mathbf{Q}}$ admits the eigen-decomposition:

$$\tilde{\mathbf{Q}} = \mathbf{V}\mathbf{\Lambda}\mathbf{U}^T, \quad [8]$$

then $\mathbf{Q}$ be written as:

$$\mathbf{Q} = (\mathbf{\Pi}^{-1/2}\mathbf{V})\mathbf{\Lambda}(\mathbf{\Pi}^{1/2}\mathbf{U})^T, \quad [9]$$

where $\mathbf{\Pi}^{-1/2}\mathbf{V}$ and $\mathbf{\Pi}^{1/2}\mathbf{U}$ are the matrices, that contain respectively the sets of left and right eigenvectors of $\mathbf{Q}$. By replacing $\mathbf{Q}$ in Eq. [5] by its expression in Eq. [9], it becomes:

$$\mathbf{P}_t = \mathbf{\Pi}^{-1/2} e^{t\tilde{\mathbf{Q}}}\, \mathbf{\Pi}^{1/2}. \quad [10]$$

Fourier Transform of the Diffusion Spectrum

Let us define the displacement spectrum $\bar{p}_t(\mathbf{r})$ over the network as the probability for a spin in the network to experience a relative vector displacement $\mathbf{r}$ for a diffusion time t. If $\mathbf{x}(0)$ and $\mathbf{x}(t)$ are the random variables that define the positions of an individual spin at time 0 and time t, respectively, then we can write:

$$\bar{p}_t(\mathbf{r}_k) = \sum_{i,j:\mathbf{x}_j - \mathbf{x}_i = \mathbf{r}_k} M_{ii}\, P_{ij}, \quad [11]$$

with $P_{ij} \triangleq (\mathbf{P}_t)_{ij}$. In other words, we say that the sum over the joint distribution $p(\mathbf{x}(t) = \mathbf{x}_j, \mathbf{x}(0) = \mathbf{x}_i) = M_{ii}P_{ij}$ is restricted to the displacements such that $\mathbf{x}(t) - \mathbf{x}(0) = \mathbf{r}_k$.

It remains for us to take the Fourier transform of the diffusion spectrum:

$$\Psi(\mathbf{q}) = \sum_k \bar{p}_t(\mathbf{r}_k) e^{\sqrt{-1}\,\mathbf{q}\cdot\mathbf{r}_k} \quad [12]$$

$$= \sum_{i,j} M_{ii}P_{ij}\, e^{\sqrt{-1}\,\mathbf{q}\cdot(\mathbf{x}_j - \mathbf{x}_i)} \quad [13]$$

$$= \mathbf{f}_\mathbf{q}^*(\mathbf{M}\mathbf{P}_t)\mathbf{f}_\mathbf{q}, \quad [14]$$

where the effect of the spatial Fourier encoding on the network is represented by the N-dimensional vector $\mathbf{f}_\mathbf{q} = [e^{\sqrt{-1}\,\mathbf{q}\cdot\mathbf{x}_1}, \ldots, e^{\sqrt{-1}\,\mathbf{q}\cdot\mathbf{x}_N}]^T$ and its Hermitian $\mathbf{f}_\mathbf{q}^*$. Substituting $\mathbf{P}_t$ Eq. [14] by its expression in Eq. [10] yields:

$$\Psi(\mathbf{q}) = \mathbf{f}_\mathbf{q}^*(\mathbf{M}\mathbf{\Pi}^{-1/2} e^{t\tilde{\mathbf{Q}}}\, \mathbf{\Pi}^{1/2})\mathbf{f}_\mathbf{q}. \quad [15]$$

If we consider the system in stationary state, $\mathbf{M} = \mathbf{\Pi}$, and therefore Eq. [15] simplifies as follows:

$$\Psi(\mathbf{q}) = (\mathbf{f}_\mathbf{q}^*\mathbf{\Pi}^{1/2}) e^{t\tilde{\mathbf{Q}}}\, (\mathbf{\Pi}^{1/2}\mathbf{f}_\mathbf{q}) \quad [16]$$

$$= \mathbf{u}_\mathbf{q}^* e^{t\tilde{\mathbf{Q}}}\, \mathbf{u}_\mathbf{q}, \quad [17]$$

where $\mathbf{u}_\mathbf{q} = \mathbf{\Pi}^{1/2}\mathbf{f}_\mathbf{q}$.

Since the eigenvalues of $\tilde{\mathbf{Q}}$ are real, by the spectral mapping theorem (11), those of $e^{t\tilde{\mathbf{Q}}}$ are real and positive, and therefore:

$$\mathbf{u}^* e^{t\,\tilde{\mathbf{Q}}}\, \mathbf{u} > 0, \quad \text{for all } \mathbf{u} \in \mathbb{C}^N \backslash \{0\} \text{ and for all } t \in \mathbb{R}^+, \quad [18]$$

which completes the proof.

On the Finite Duration of Diffusion Encoding Gradients

As just shown, the narrow pulse approximation allows us to easily understand the intrinsic Fourier relationship between the MR signal and the underlying water mobility that is a mirror of the tissue compartmentation. However, in practice, the duration of the diffusion-encoding gradient is not negligible compared to the diffusion time Δ (i.e., $\delta \approx \Delta$), so the formalism developed above must be reexamined. Interestingly, the reconstruction described in Eq. [4] still remains valid with non-infinitesimal diffusion-encoding gradients. In particular, the MR signal related to diffusion remains positive (see Appendix). Nevertheless, as shown by Mitra and Halperin (12), the interpretation of the diffusion spectrum, $\bar{p}_\Delta(\mathbf{r})$, must change slightly. In this case, the vector $\mathbf{r}$ must be interpreted as the δ-averaged relative spin displacement. This means that $\mathbf{r}$ describes the displacement of the spin mean position within the time interval $[0, \delta]$ relative to mean position in the interval $[\Delta, \delta + \Delta]$. As a consequence, the diffusion distance is usually slightly underestimated and the separation power diminishes. The global shape of the function remains and, in the end, the interpretation is substantively unchanged.

DSI is a 6D MRI Technique

The effect of embedding diffusion-encoding gradients into a classic spin-echo MRI experiment is that new dimensions are added to the sampling space. While k-space samples the spatial postion, q-space samples the space of the spin displacements. In complete analogy to classic k-space MRI, DSI samples k- and q-space at the same time, yielding a true 6D imaging technique of position and displacement.

MATERIALS AND METHODS

MR Experiments

Three data sets were acquired at 3T with an Allegra headscanner using a single-shot echo-planar MRI acquisition with a spin-echo pulse sequence augmented by diffusion-encoding gradient pulses, and incorporating two π RF pulses to minimize the effects of eddy currents (13). At each location, diffusion-weighted images were acquired for $N = 515$ values of q-encoding, comprising in q-space

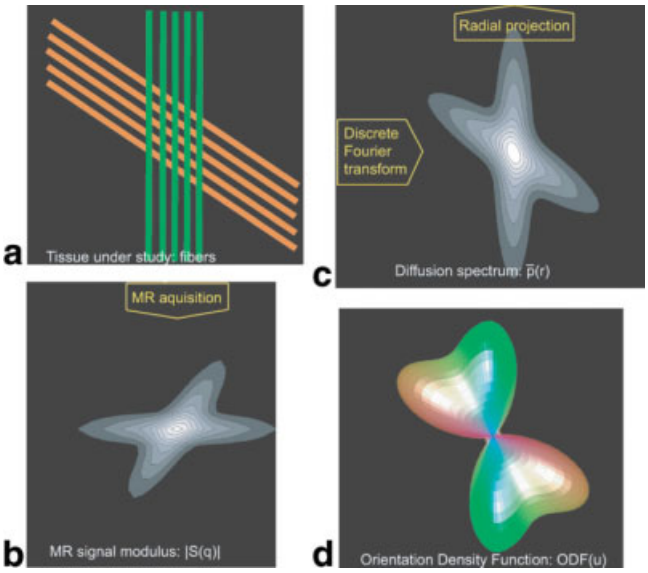

FIG. 1. DSI reconstruction scheme. **a:** Tissue in a voxel under study. Here the tissue is represented by two populations of fibers that cross. **b:** Through the MR acquisition scheme the signal $|S_\Delta(\mathbf{q})|$ is sampled. **c:** In order to reconstruct the diffusion spectrum, the 3D discrete Fourier transform is taken. **d:** To simplify the representation of an imaging slice, the angular structure of diffusion is represented as a polar plot of the radial projection (orientation distribution function). The color coding corresponds to the orientation of diffusion (green: vertical diffusion; red: transverse diffusion).

the points of a cubic lattice within the sphere of five lattice units in radius (Fig. 1b):

$$\mathbf{q} = a\mathbf{q}_x + b\mathbf{q}_y + c\mathbf{q}_z, \qquad [19]$$

with a, b, c integers and $\sqrt{a^2 + b^2 + c^2} \leq 5$. $\mathbf{q}_x$, $\mathbf{q}_y$,and $\mathbf{q}_z$ denote the unit phase modulations in the respective coordinate directions. The diffusion spectrum was then reconstructed by taking the discrete 3D Fourier transform of the signal modulus (Fig. 1c). The signal is premultiplied by a Hanning window before Fourier transformation in order to ensure a smooth attenuation of the signal at high $|\mathbf{q}|$ values. The imaging parameters specific to each of the three data sets are summarized in Table 1. The typical scheme for brain imaging uses gradient pulses of peak intensity $g_{\max} = 40$ mT/m, duration $\delta = 60$ms with experimental mixing time $\Delta = 66$ ms, thus achieving a nominal isotropic resolution $r_{\min} = q_{\max}^{-1} = 10$ μm of FOV $r_{\max} = q_{\min}^{-1} = 50$ μm[1], and a $b_{\max} = 17000$ s/mm^2.

Since we are mainly interested in the angular structure of the diffusion spectrum, we further simplified the data by taking a weighted radial summation of $\bar{p}_\Delta(\mathbf{r})$:

$$\mathrm{ODF}(\mathbf{u}) = \int_{\mathbb{R}^+} \bar{p}_\Delta(\rho\mathbf{u})\rho^2 d\rho, \quad \text{with } \|\mathbf{u}\| = 1. \qquad [20]$$

This defines the orientation distribution function (ODF), which measures the quantity of diffusion in the direction of the unit vector $\mathbf{u}$ (Fig. 1d).

For some data we reconstructed the estimated DT by least-square estimation using the 27 samples that lay on the 3D Cartesian grid in a ball of radius $b_{\max} = 2000$ s/mm^2.

Sample Preparation and Subjects

Two normal subjects were scanned in compliance with the MGH Institutional Review Board (IRB), the and confidentiality was maintained in compliance with the Health Insurance Portability and Accountability Act of 1996 (HIPPA). Fresh, nonfrozen beef tongue was placed without any other treatment in the head coil, and the sample was held at room temperature during the acquisition.

RESULTS

DSI in a coronal plane of the brain of a normal volunteer is shown in Figs. 2 and 3. Figure 2 compares the signal

[1]Due to non-infinitesimal diffusion-gradient durations, the true $r_{\min}$ and $r_{\max}$ are expected to be slightly larger.

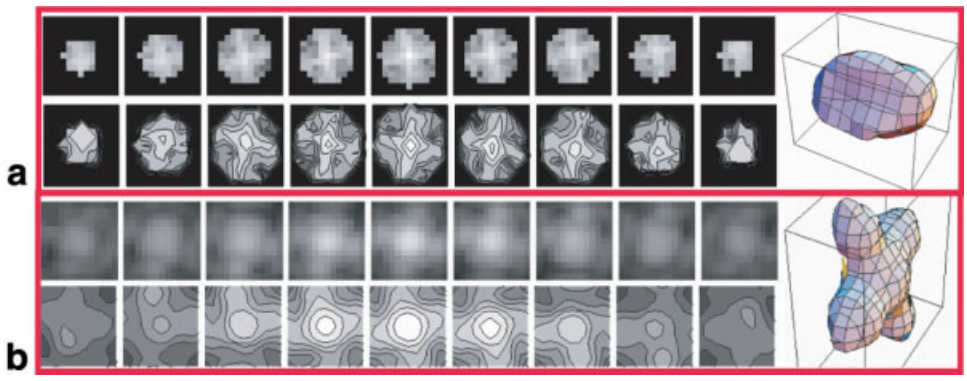

FIG. 2. Spectral data for one voxel within the brainstem demonstrates heterogeneous diffusion anisotropy. **a:** Raw data $|S_\Delta(\mathbf{q})|$ are shown as a set of contour plots for consecutive 2D planes in q-space. These data show an intensity maximum with the shape of a tilted "X," the two lobes of which suggest contributions of two orientational fiber populations within this voxel. **b:** The diffusion spectrum $\bar{p}_\Delta(\mathbf{r})$ is reconstructed by discrete 3D Fourier transform of the raw data and is represented by 2D and 3D contour plots (the latter is a locus of points r such that $\bar{p}_\Delta(\mathbf{r})$ = constant. This 3D displacement spectrum shows two well-defined orientational maxima.

Table 1
Summary of Acquisition Parameters

Data set	Coronal brain slice	Para-sagital brain block	Fresh beef tongue
Technique	Single-shot, single slice	Single-shot, multi-slice	Single-shot, single slice
Coil	Single channel quadrature head coil	Single channel quadrature head coil	Single channel quadrature head coil
Matrix size × number of slices	64 × 64 × 1	64 × 64 × 14	64 × 64 × 1
Voxel dimension [mm]	3.6 × 3.6 × 3.6	3.2 × 3.2 × 3.2	4 × 4 × 4
EPI readout [ms]	32	32	32
TE/TR [ms]	156/3000	156/3000	125/3000
Δ/δ [ms]	66/60	66/60	50/45
g_{max} [mT/m]	40	40	40
b_{max} [s/mm^2]	17000	17000	8000
Acquisition time [min]	~25	~25	~25

$|S_\Delta(\mathbf{q})|$ and its 3D Fourier transform, the diffusion spectrum $\bar{p}_\Delta(\mathbf{r})$, for a voxel within the brainstem. Here the signal $|S_\Delta(\mathbf{q})|$ is clearly multimodal and far from Gaussian, and its spectrum has 3D directional maxima orthogonal to those of $|S_\Delta(\mathbf{q})|$.

Figure 3 illustrates the DSI experiment on the whole coronal slice that includes elements of the corticospinal tract and the pontine decussation of the middle cerebellar peduncles. While Fig. 3a shows the DT image reconstructed from the DSI data, Fig. 3b and c zoom in on the brainstem and centrum semiovale. At each voxel is shown the ODF represented as a spherical polar plot and colored according to local orientations. In Fig. 3b we see that while many voxels show spectral maxima of single orientations, corresponding to the axial corticospinal tract (blue) and mediolateral pontocerebellar fibers (green), voxels within the intersection of these tracts at once show both orientational maxima. Figure 3c shows a portion of the centrum semiovale, including elements of the corona radiata, superior longitudinal fasciculus, and corpus callosum, that are respectively of axial, anteroposterior, and mediolateral orientations. Diffusion spectra demonstrate the corresponding orientational maxima, and in particular include voxels that exhibit two- and three-way coincidences of these tracts. Note that the DT of a voxel showing a symmetric three-way crossing corresponds to a DT of low anisotropy (see yellow circle).

The orientational maxima of local cerebral diffusion can be used to identify in every voxel the axonal orientation of several fiber populations. In Fig. 4 we imaged a parasagittal brain block and used sticks to represent those maxima. We can easily identify callosal fibers in the center of the image (magenta to orange). When they extend laterally, they partially cross the cingulate fiber bundle that runs anteroposteriorly in green. In the upper part of the image, blue sticks correspond to callosal and pyramidal fibers that project into the apical cortex.

The application of DSI to muscular tissues is illustrated by ex vivo studies of the tongue. The coupled contraction of the intrinsic muscles of the tongue (a sheath of conventional skeletal muscle of longitudinal orientation, and a core of orthogonal interlaced fiber bundles of the transversus and verticalis muscles) enables the tongue to stiffen, deviate, and protrude in opposition to the longitudinalis. This architecture is clearly delineated in DSI of a bovine tongue (Fig. 5). While spectra at superficial locations show single longitudinally-oriented maxima, corresponding to the longitudinalis muscle, the core voxels usually show two approximately orthogonal maxima corresponding to the transversus and verticalis muscles.

DISCUSSION

The positivity of the Fourier transforms of diffusion spectra of general diffusion processes described above generalizes familiar facts. If diffusion is homogeneous and unrestricted (i.e., Gaussian), then its displacement spectrum is stable under self-convolution (Levy stable) and thus has a positive Fourier transform. If diffusion is restricted and fully evolved, then its displacement spectrum tends to the autocorrelation of the restriction geometry (14), a function whose transform again is positive. The present approach encompasses the general situation expected in vivo, in which microenvironments of distinct anisotropic diffusivities exchange spins across a continuum of time scales. In other words, depending on the allowed diffusion time Δ, the water molecules have more or less time to explore the tissue environment, and accordingly influence the diffusion spectrum. Let us consider a simple model made of a connected porous system, following the image given by Callaghan (8). Intuitively, when the diffusion time is such that the average diffusion distance is much smaller than the restriction geometry, the diffusion spectrum is an isotropic Gaussian function. At intermediate time scales, spins are given a chance to explore fully the local compartment without exchanging significantly between adjacent pores. Hence, the diffusion spectrum captures the additive effects of the pore shape autocorrelations. At longer time scales, spin exchange equilibrates successively with more distant compartments that generate successive cross-correlation terms between pores. If these compartments have different shapes and/or orientations, the appearance of cross terms will result in a blurrier diffusion spectrum. This suggests that there must exist an optimal diffusion time for which the diffusion spectrum is orientationally the sharpest.

The study of diffusion by the quite general formalism developed here, which also encompasses the more commonly used finite element model, naturally highlights the essential features of the system that contribute to the positivity of the diffusion contrast. We see that positivity relies critically on the facts that the system is in equilib-

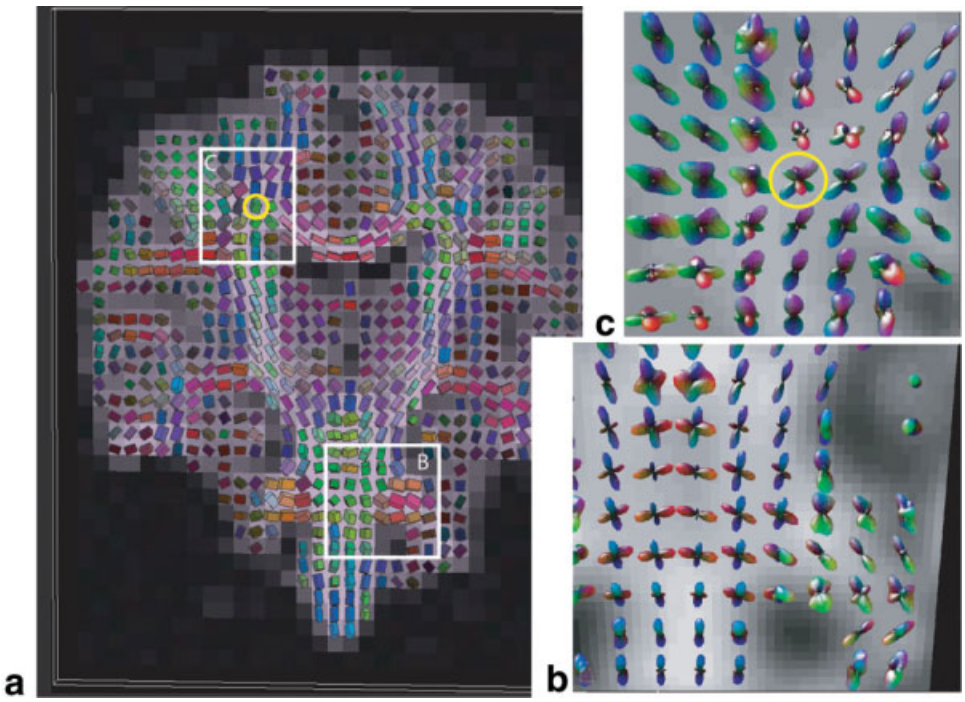

FIG. 3. Cerebral DSI of normal human subjects. **a:** The complete coronal brain slice under study. Diffusion is represented with a tensor fit from the DSI data. Tensors are represented as boxes shaped by the eigenvalues and eigenvectors, and color-coded based on leading eigenvector orientation (blue: axial; red: transverse; green: anteroposterior orientation). **b:** Zoom image of the brainstem. Diffusion spectra are represented as polar plots of the ODFs that are color-coded depending on diffusion orientation. Here, the corticospinal tract contributes spectral maxima of axial orientation (blue lobes along the vertical axis) and the pontine decussation of the middle cerebellar peduncle contributes horizontally (green lobes crossing at center). Many local spectra show contributions of both structures. **c:** This image shows the centrum semiovale and contains elements of the corticospinal tract (blue), corpus callosum (green), and superior longitudinal fasciculus (red), including voxels with two- and three-way intersections of these components. Orientational correspondence between tensor and spectral data is best at locations with simple unimodal spectra, while locations with multimodal diffusion spectra correspond to relatively isotropic DTs.

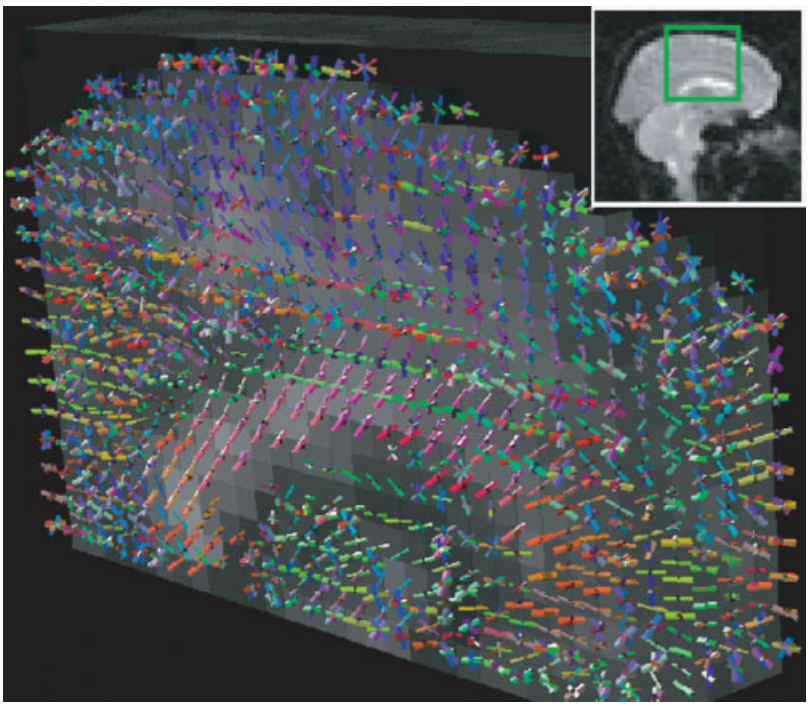

FIG. 4. Brain map of orientational diffusion maxima. Colored sticks are used to represent the local maxima of diffusion in every voxel. They are used to identify the local axonal orientation of several fiber populations. Callosal fibers can be seen in the center of the image (magenta to orange indicating transverse orientation). More laterally, they cross partially the cingulate fiber bundle that runs anteroposteriorly (green). In the upper part of the image, blue sticks of axial orientation correspond to callosal and pyramidal fibers that project into the apical cortex.

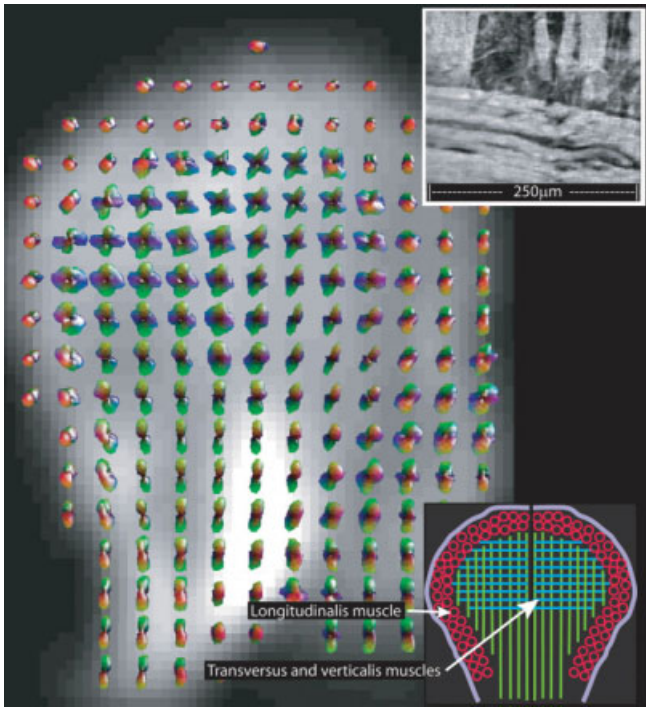

FIG. 5. MRI of complex muscle. In this image we see as DSI image of the bovine tongue, a coronal slice with 4-mm resolution, represented as polar plots of the ODFs. The longitudinalis muscle seen at the superior surface of the tongue shows a single through-plane orientation (red). The core of the tongue shows the intersecting elements of the transversus (blue) and verticalis muscles (green), which often coexist within one voxel. On the top right, an electron micrograph illustrates the intersecting fascicles at the micrometric level (courtesy of Vitaly Napidow and Richard Gilbert).

rium, no net fluxes occur, and the considered voxel is isolated from its neighbors. Although these constraints should be respected in most voxels of the current in vivo diffusion experiments, in some instances the preconditions of positivity may be violated. Indeed, some instances could induce a phase-shift when such processes have sufficient spatial coherence to produce significant net orientational asymmetry at the scale of one voxel. For example, spin flux related to perfusion (15), or virtual flux produced by inhomogeneous relaxation, as well as significant asymmetric mass exchange at voxel boundaries—possibly occurring with very high resolution imaging (e.g., the submillimetric voxel model of Liu et al. (16))—may violate positivity. In simulation, initializing the system in a nonstationary distribution would be an additional cause for artifactual phase-shift as spins redistribute toward the equilibrium. In the absence of positivity, autocorrelations of the present diffusion spectra may be reconstructed from the square of the signal. Such autocorrelations will appear less sharp than the displacement spectra, owing to terms arising from cross-correlations between distinct spectral components, and would not be linear functions of the signal.

Through this general formalism, we have also shown that using long diffusion-encoding gradients ($\delta \approx \Delta$) neither precludes the positivity condition nor impairs significantly the interpretation of the diffusion spectrum. While the object size estimation (17) may be problematic with the use of a non-infinitesimal diffusion gradient, the only effect on orientation inference is expected to be a decrease in separation power due to some blurring.

The analysis of tissue fiber architecture with DSI is based on the familiar principle that water diffusion in biological materials is least restricted in directions parallel to fibers (18). When considering voxels of single fiber population, the signal $S(\mathbf{q})$ in 3D q-space is bright over a 2D disc, perpendicular to the fiber direction. After 3D Fourier transformation, the resulting diffusion spectrum concentrates along a line corresponding to the fiber direction. With two crossing fiber populations, we move from two intersecting discs in q-space to two lines of maximum intensity in the reciprocal space. In the context of mapping fiber orientation, the 3D Fourier transform of the MR signal has two obvious consequences: First, it enhances the SNR by projecting the samples in a disc into a line, concentrating the energy of the data in a smaller volume fraction of a 3D space. This is just as in spectroscopy where the Fourier transform concentrates the (long time) FID in a (band-limited) spectral peak. Second, whereas in the multicomponent case the minima and maxima of two crossing discs in q-space are meaningless, after 3D Fourier transform those maxima correspond to clear fiber orientations (Figs. 1 and 2). Like tensor imaging, DSI associates fiber orientations with directions of maximum diffusion, but it now admits the possibility of having multiple directions at each location. Histologically, neural tract and muscle intersections such as the examples (Figs. 3–5) above consist of interdigitating multicellular fascicles that are tens to hundreds of microns in diameter. While DT imaging (DTI) of such architectures would essentially have to resolve individual fascicles and would therefore require micrometric resolution, DSI, as validated in Ref. 19, overcomes this limitation by defining orientational coherence without individually resolving constituent fascicles. Such DSI requires only sufficient spatial resolution as to limit intravoxel dispersion of fiber orientations that belong to a neural tract produced by bending, splaying, and twisting.

Determining the nominal angular resolution from the DSI sample density is a straightforward procedure. Assuming that the gradient vectors are isotropic across a sphere:

$$\sqrt{\frac{4\pi}{S}} = \theta \qquad [21]$$

where S is the number of evenly spaced samples, and θ is the angular resolution in radians. In our sampling scheme, some of the sample vectors are colinear with the origin, and thus we have 411 samples over the unit sphere. This means that our acquisition of 515 samples can provide, at best, an angular resolution of 10° when localizing and separating fiber bundles. Other factors will blur that ideal resolution, including the angular heterogeneity of fiber populations, the diffusion contrast, diffusion mixing time, and the signal-to-noise ratio (SNR) of the acquisition.

The fiber orientation separation power relies critically on the maximal sampling radius. While extending the maximal sampling radius above b-values of 18000 s/mm^2 is not expected to improve accuracy (20), not going far

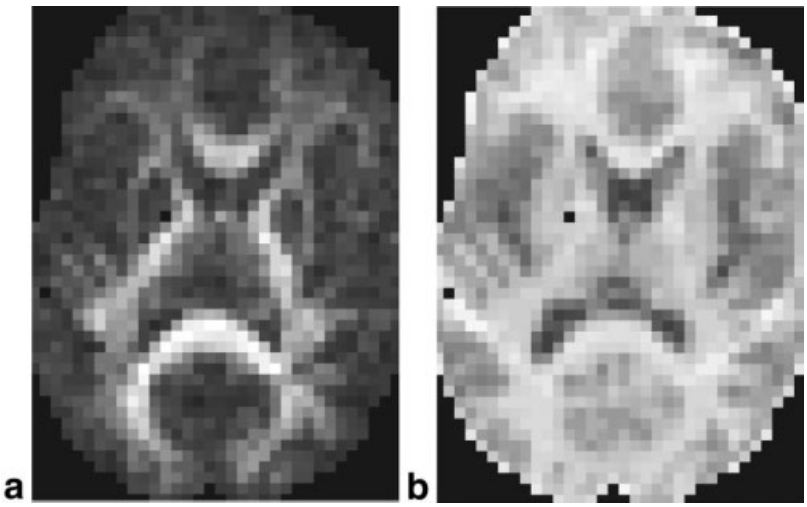

FIG. 6. **a:** FA map of a brain slice computed by reconstruction of the DT from the DSI data. **b:** The negative of the kurtosis computed on the diffusion spectrum. Note the correlation between both images ($r = 0.6$).

enough in q-space will limit the angular contrast. In our experience, a maximal b-value of 12000–18000 s/mm^2 appears to be adequate for resolving well known areas of crossing fibers, such as the brainstem and centrum semiovale.

DTI is a widely used imaging technique that is based on a Gaussian model. Since we are now able to do model-free imaging by sampling without major a priori assumptions about the diffusion function using DSI, it is worthwhile to understand the relationship between these techniques. We mentioned above that the MR signal $S_\Delta(\mathbf{q})$ can be seen as the characteristic function of the random variable $\mathbf{r}$, which describes the average spin displacement in a voxel (21). The first few terms of its 3D Taylor expansion around zero are:

$$\ln[S_\Delta(\mathbf{q})/S_0] = 0 + i\mathbf{q}^T E(\mathbf{r}) - \frac{1}{2}\mathbf{q}^T[E(\mathbf{r}\mathbf{r}^T) - E(\mathbf{r})E(\mathbf{r})^T]\mathbf{q} + O(|\mathbf{q}|^3), \quad [22]$$

where $E(\cdot)$ means expectation, and $[E(\mathbf{r}\mathbf{r}^T) - E(\mathbf{r})E(\mathbf{r})^T]$ is the covariance matrix. As shown above, we can take into account that the signal is a centered and even function (odd terms are zero). To move to the DT model, we see from the above expression that we need to neglect the terms of order higher than 2. This can be done if i) the wave vector $\mathbf{q}$ is small ($\mathbf{q}^T E(\mathbf{r}\mathbf{r}^T)\mathbf{q} \ll 1$ or ii) diffusion is Gaussian (moments of order higher than 2 are zero). We then can rewrite Eq. [22] in the following form:

$$S_\Delta(\mathbf{q})/S_0 = e^{-(1/2)\mathbf{q}^T E(\mathbf{r}\mathbf{r}^T)\mathbf{q}} \quad [23]$$

$$= e^{-\Delta\mathbf{q}^T\mathbf{D}\mathbf{q}}, \quad [24]$$

where the DT $\mathbf{D}$ is defined by the Einstein relation ($E(\mathbf{r}\mathbf{r}^T) = 2\Delta\mathbf{D}$) and we are back to the classic DTI formula (22). In brain tissue, we expect the first condition to be satisfied when b-values are less than 1000 s/mm^2 and the second condition to be satisfied in regions that exhibit single fiber orientation. A Taylor expansion suggests a simple way to measure non-Gaussianity (23) by considering the multivariate kurtosis β_2 (24), a function of the fourth-order moment of the diffusion function. Interestingly, the image of $-\beta_2$ of a brain slice (Fig. 6b) looks very similar to the DTI-based fractional anisotropy (FA) map (Fig. 6a, correlation coefficient, $r = 0.6$). This relation provides us with a new interpretation of the meaning of FA. High FA can be interpreted as brain areas in which the anisotropic Gaussian model is a good approximation and suggests unimodal fiber orientations. Conversely, low FA occurs precisely where kurtosis is high and corresponds to regions of complex fiber architecture. We therefore need to interpret DTI images with care when neither of the above conditions is satisfied. It is also worthwhile to note that in Eq. [21] the moments can be expressed in terms of DTs of corresponding order, thus bringing up the generalized DT formalism developed by Liu et al. (16).

New techniques called "high angular resolution methods" have recently emerged. They are all based on the same principle, which consists of acquiring a large number of diffusion-weighted samples of constant b-values distributed over a spherical shell. The ODFs are then reconstructed by various algorithms. Optimization schemes (as in Refs. 25 and 26) or direct reconstructions (as in q-ball imaging (27)) are used. In the context of q-space imaging, we notice that in the same way that DTI and its associated Gaussian model can be seen as a low-pass approximation of the evolved diffusion function, sampling a sphere of constant b-value at high angular resolution is equivalent to high-pass-filtering the diffusion spectrum. The problem is then to recover the exact ODF from a band-limited signal, which requires clever a priori assumptions.

Cohen and Assaf (17) and Avram et al. (28) studied simple tubular tissue geometries by sampling in q-space a line perpendicular to the main tissue axis. This allowed them to retrieve information about the diameter of the tubular shape by studying the diffraction patterns or by computing the 1D Fourier transform of the acquired 1D MR signal. Again in the context of DSI, 1D q-space imaging can be understood as a projection imaging technique (i.e., the 1D Fourier transform along a line in q-space is the projection of the 3D diffusion spectrum on that same line). Like all projection imaging techniques, the mapping be-

tween the 3D shape and its 1D projection is not necessarily one to one (e.g., the biexponential decay could be related to two compartments of different diameters but also of different orientation or permeability). This type of imaging, though straightforward in simple geometries, might raise intractable interpretation problems if attempted on tissues with intra-voxel orientational heterogeneity like the brain.

Based on the observation that diffusion contrast is positive, we have described DSI as a generalized model-free diffusion MRI technique. DSI is a 6D imaging technique that makes fiber orientation imaging a conventional MRI technique, in the sense that it is faced with the standard MRI limitations (such as SNR and angular resolution) and is based on minor and well-supported assumptions. We have shown that DSI has the capacity to unravel structural information from tissue architecture as complex as micrometric interdigitating muscle fibers and crossing axonal fibers in the central nervous system, without the need for a priori information or ad hoc models.

APPENDIX

As noted above, the diffusion gradient pulses in the Stejskal-Tanner experiment are indeed of finite duration. Therefore, we must verify that even in this case the MR signal is guaranteed to be positive. The framework presented in the Theory section above remains valid, which means that the system is isolated and homogenous, and the diffusion process in stationary state. We remember that the MR signal can be seen as proportional to the expected value of the dephasing due to spin motion (Eq. [2]). However, the phase is no longer proportional to the dot product between the *q*-wave vector and the relative spin displacement. The expression $\phi = \mathbf{q} \cdot \mathbf{r}$ needs to be reformulated. We use the formalism developed by Caprihan et al. (29), who wrote the dephasing induced by spin motion as a function of a multiplet of infinitesimal narrow pulses. Time is discretized regularly at intervals $\xi = (\Delta + \delta)/2L$ and indexed by $l \in \{-L, -L + 1, \ldots, L\}$, where $-L$ and -1 are respectively the times at the beginning and end of the first diffusion gradient, 0 corresponds to the time of the π RF-pulse, $+1$ and $+L$, correspond respectively to the beginning and end of the second diffusion gradient. This yields the simple expression

$$\phi = \mathbf{q} \cdot \sum_{l=-L}^{L} a_l \mathbf{x}(l) \qquad [25]$$

with $a_l = -a_{-l}$ and $a_0 = 0$.

Mathematically, we can consider $\{\mathbf{x}(l)\}_{-L \le l \le L}$ to be the embedded discrete MC of the diffusion process $\{\mathbf{x}(t)\}_{t>0}$ described. It has a transition matrix $\mathbf{P}_\xi$ and is reversible because it satisfies the detailed balance equations (9). In this context each $\mathbf{x}(l)$ is a random variable defined on the set of the network vertices, and represents the position of the random walk at time index l. We call $\Sigma_{l=-L}^{L} a_l \mathbf{x}(l)$ with $a_l = -a_{-l}$ and $a_0 = 0$ a bipolar balanced random sum.

To convince ourselves that the MR signal even with finite-duration gradient pulses is real and positive, we have to verify that for a reversible discrete homogenous MC $\{\mathbf{x}(l)\}_{-L \le l \le L}$ of positive transition matrix $\mathbf{P}_\xi$ and in stationary state, the function

$$\Psi(\mathbf{q}) = E(e^{\sqrt{-1}\,\mathbf{q}\cdot\Sigma_{l=-L}^{L} a_l \mathbf{x}(l)}), \qquad [26]$$

where $a_l = -a_{-l}$ and $a_0 = 0$ is real and positive for all $\mathbf{q} \in \mathbb{R}^3$.

We start with the function defined in Eq. [26]. Without loss of generality and for notational simplicity, we choose $a_l = -a_{-l} = 1$. The MC is in stationary state and is reversible (9). Therefore, it is possible to express $\Psi(\mathbf{q})$ as the expectation of the product of two conditional expectations [2] by time reversal of the first half of the MC. We thus have

$$\begin{aligned}\Psi(\mathbf{q}) &= E(e^{\sqrt{-1}\,\mathbf{q}\cdot\Sigma_{l=-L}^{L} a_l \mathbf{x}(l)}) \\ &= E(E(e^{-\sqrt{-1}\,\mathbf{q}\cdot\Sigma_{l=-L}^{-1} \mathbf{x}(l)} | \mathbf{x}(-1)) E(e^{\sqrt{-1}\,\mathbf{q}\cdot\Sigma_{l=1}^{L} \mathbf{x}(l)} | \mathbf{x}(1))), \qquad [27]\end{aligned}$$

where the outer expectation is taken with respect to the joint distribution $p(\mathbf{x}(1), \mathbf{x}(-1))$.

By analogy with the Theory section above, we redefine an *N*-dimensional vector $\mathbf{f}_\mathbf{q} = [f_1, \ldots, f_N]^T$ such that

$$f_j = E(e^{\sqrt{-1}\,\mathbf{q}\cdot\Sigma_{l=1}^{L} \mathbf{x}(l)} | \mathbf{x}(1) = \mathbf{x}_j). \qquad [28]$$

$f_j$represents the value, which the second conditional expectation of Eq. [28] takes knowing that the value of the chain at time is $l = 1$ is $\mathbf{x}_j$. It remains for us to express the Hermitian vector $\mathbf{f}_\mathbf{q}^* = [\bar{f}_1, \ldots, \bar{f}_N]$ in terms of the values of the first conditional expectation of Eq. [27]. This is possible because the forward half chain $\{\mathbf{x}(l)\}_{1 \le l \le L}$ given $\mathbf{x}_1$ is equally distributed as the backward half chain $\{\mathbf{x}(-l)\}_{-L \ge -l \ge -1}$ given $\mathbf{x}_{-1}$. We thus have

$$\begin{aligned}\bar{f}_i &= E(e^{-\sqrt{-1}\,\mathbf{q}\cdot\Sigma_{l=1}^{L} \mathbf{x}(l)} | \mathbf{x}(1) = \mathbf{x}_i) \\ &= E(e^{-\sqrt{-1}\,\mathbf{q}\cdot\Sigma_{l=-L}^{-1} \mathbf{x}(l)} | \mathbf{x}(-1) = \mathbf{x}_j). \qquad [29]\end{aligned}$$

We rewrite Eq. [27] in matrix form by using the newly defined vectors $\mathbf{f}_\mathbf{q}$ and $\mathbf{f}_\mathbf{q}^*$ and by noticing that in the stationary state the joint distribution $p(\mathbf{x}(1) = \mathbf{x}_j, \mathbf{x}(-1) = \mathbf{x}_i) = \Pi_{ii} P_{ij}$, with $P_{ij} = (\mathbf{P}_{2\xi})_{ij}$, hence:

$$\Psi(\mathbf{q}) = \mathbf{f}_\mathbf{q}^* (\mathbf{\Pi} \mathbf{P}_{2\xi}) \mathbf{f}_\mathbf{q} \qquad [29]$$

$$= (\mathbf{f}_\mathbf{q}^* \mathbf{\Pi}^{1/2}) e^{2\xi\tilde{\mathbf{Q}}} (\mathbf{\Pi}^{1/2} \mathbf{f}_\mathbf{q}), \qquad [30]$$

by replacing in Eq. [29] $\mathbf{P}_{2\xi}$ with Eq. [10]. It follows that $\Psi(\mathbf{q}) > 0$ since we have seen that $e^{2\xi\tilde{\mathbf{Q}}}$ is a positive operator.

[2]For two random variables *A* and *B* the conditional expectation $E(A|B = b)$ is the value of the expectation of *A* knowing that *B* takes the value *b*..

ACKNOWLEDGMENTS

The authors thank David Tuch, Mette Wiegell, Vitaly Napidow, and Richard Gilbert for many helpful discussions, and Jean-Philippe Thiran and Reto Meuli for their support.

REFERENCES

1. Le Bihan D. Looking into the functional architecture of the brain with diffusion MRI. Nat Rev Neurosci 2003;4:469–480.
2. Tseng WY, Reese TG, Weisskoff RM, Brady TJ, Wedeen VJ. Myocardial fiber shortening in humans: initial results of MR imaging. Radiology 2000;216:128–139.
3. Tseng WY, Wedeen VJ, Reese TG, Smith RN, Halpern EF. Diffusion tensor MRI of myocardial fibers and sheets: correspondence with visible cut-face texture. J Magn Reson Imaging 2003;17:31–42.
4. Wedeen VJ, Reese TG, Napadow VJ, Gilbert RJ. Demonstration of primary and secondary muscle fiber architecture of the bovine tongue by diffusion tensor magnetic resonance imaging. Biophys J 2001;80:1024–1028.
5. Mori S, van Zijl PC. Fiber tracking: principles and strategies—a technical review. NMR Biomed 2002;15:468–480.
6. Wiegell MR, Larsson HB, Wedeen VJ. Fiber crossing in human brain depicted with diffusion tensor MR imaging. Radiology 2000;217:897–903.
7. Stejskal E, Tanner J. Spin diffusion measurements—spin echoes in presence of a time-dependent field gradient. J Chem Phys 1965;42:288–300.
8. Callaghan PT. Principles of nuclear magnetic resonance microscopy. Oxford: Clarendon Press; 1991. 494 p.
9. Brémaud P. Markov chains Gibbs fields, Monte Carlo simulation, and queues. New York: Springer; 1999. 444 p.
10. Le Bihan D, Turner R. Intravoxel incoherent motion imaging using spin echoes. Magn Reson Med 1991;19:221–227.
11. Horn RA, Johnson CR. Matrix analysis. Cambridge: Cambridge University Press; 1985. XIII, 561 p.
12. Mitra P, Halperin B. Effects of finite gradient-pulse widths in pulsed-field-gradient diffusion measurements. J Magn Reson Ser A 1995;113:94–101.
13. Reese TG, Heid O, Weisskoff RM, Wedeen VJ. Reduction of eddy-current-induced distortion in diffusion MRI using a twice-refocused spin echo. Magn Reson Med 2003;49:177–182.
14. Cory D, Garroway A. Measurements of translational displacement probabilities by nmr—an indicator of compartmentation. Magn Reson Med 1990;14:435–444.
15. Le Bihan D. Diffusion and perfusion magnetic resonance imaging: applications to functional MRI. Philadelphia: Lippincott Williams & Wilkins; 1995.
16. Liu C, Bammer R, Acar B, Moseley M. Characterizing non-Gaussian diffusion by using generalized diffusion tensors. Magn Reson Med 2004;51:924–937.
17. Cohen Y, Assaf Y. High b-value q-space analyzed diffusion-weighted MRS and MRI in neuronal tissues—a technical review. NMR Biomed 2002;15:516–542.
18. Beaulieu C. The basis of anisotropic water diffusion in the nervous system—a technical review. NMR Biomed 2002;15:435–455.
19. Lin CP, Wedeen VJ, Chen JH, Yao C, Tseng WY. Validation of diffusion spectrum magnetic resonance imaging with manganese-enhanced rat optic tracts and ex vivo phantoms. Neuroimage 2003;19:482–495.
20. Meca C, Chabert S, Le Bihan D. Diffusion MRI at large b values: what's the limit? In: Proceedings of the 12th Annual Meeting of ISMRM, Kyoto, Japan, 2004. p 1196.
21. Resnick SI. A probability path. Boston/Basel: Birkhauser; 1999. XII, 453 p.
22. Le Bihan D. Molecular diffusion nuclear magnetic resonance imaging. Magn Reson Q 1991;7:1–30.
23. Chabert S, Meca C, Le Bihan D. Relevance of the information about the diffusion distribution in vivo given by kurtosis in q-space imaging. In: Proceedings of the 12th Annual Meeting of ISMRM, Kyoto, Japan, 2004. p 1238.
24. Mardia KV, Kent JT, Bibby JM. Multivariate analysis. London: Academic Press; 1979. XV, 521 p.
25. Tuch DS, Reese TG, Wiegell MR, Makris N, Belliveau JW, Wedeen VJ. High angular resolution diffusion imaging reveals intravoxel white matter fiber heterogeneity. Magn Reson Med 2002;48:577–582.
26. Jansons K, Alexander D. Persistent angular structure: new insights from diffusion MRI data. Dummy version. Lect Notes Comput Sci 2003;2732:672–683.
27. Tuch DS, Reese TG, Wiegell MR, Wedeen VJ. Diffusion MRI of complex neural architecture. Neuron 2003;40:885–895.
28. Avram L, Assaf Y, Cohen Y. The effect of rotational angle and experimental parameters on the diffraction patterns and micro-structural information obtained from q-space diffusion NMR: implication for diffusion in white matter fibers. J Magn Reson 2004;169:30–38.
29. Caprihan A, Wang L, Fukushima E. A multiple-narrow-pulse approximation for restricted diffusion in a time-varying field gradient. J Magn Reson Ser A 1996;118:94–102.